Review of Scientific Instruments

Single-pass non-destructive electronic detection of charged particles

Cite as: Rev. Sci. Instrum. **90**, 113301 (2019); https://doi.org/10.1063/1.5110988
Submitted: 22 May 2019 . Accepted: 14 October 2019 . Published Online: 01 November 2019

Markus Kiffer, Stefan Ringleb, Nils Stallkamp, Béla Arndt, Ilya Blinov, Sugam Kumar, Stefan Stahl, Thomas Stöhlker, and Manuel Vogel

Review of Scientific Instruments ARTICLE scitation.org/journal/rsi

Single-pass non-destructive electronic detection of charged particles

Cite as: Rev. Sci. Instrum. 90, 113301 (2019); doi: 10.1063/1.5110988
Submitted: 22 May 2019 • Accepted: 14 October 2019 •
Published Online: 1 November 2019

Markus Kiffer,[1,a)] Stefan Ringleb,[1] Nils Stallkamp,[1,2] Béla Arndt,[3] Ilya Blinov,[4] Sugam Kumar,[5] Stefan Stahl,[6] Thomas Stöhlker,[2,7] and Manuel Vogel[2]

AFFILIATIONS

[1]Friedrich Schiller-Universität Jena, 07743 Jena, Germany
[2]GSI Helmholtzzentrum für Schwerionenforschung, 64291 Darmstadt, Germany
[3]Goethe-Univerisität Frankfurt, 60629 Frankfurt, Germany
[4]Technische Universität Darmstadt, 64289 Darmstadt, Germany
[5]Inter-University Accelerator Centre, 110067 New Delhi, India
[6]Stahl Electronics, 67582 Mettenheim, Germany
[7]Helmholtz-Institut Jena, 07743 Jena, Germany

[a)]**Electronic mail:** markus.kiffer@uni-jena.de

ABSTRACT

We have devised an experimental method and apparatus for the simultaneous nondestructive determination of the absolute ion number, ion kinetic energy, and length of bunches of charged particles. We have built and operated a corresponding electronic detector that is based on induced charges and their subsequent low-noise amplification at cryogenic temperatures. We have performed measurements with bunches of low-energy highly charged ions from an electron-beam ion source that show the capability of the methods and their implementation. We discuss requirements for, and applications of, such detectors with a particular view on the obtainable information and their sensitivity.

I. INTRODUCTION

There is substantial interest in particle beam diagnostics that does not destruct or change the properties of the beam in question. This is true, in particular, for experiments with rare species, when duty cycles are low or when the properties of subsequent particle bunches need to be known individually. In storage-ring physics, Schottky-type electronic pick-ups have been brought forward that make use of the large number of equally spaced signals induced by a particle bunch which revolves at high rates in the ring. This allows sensitivities on the level of single particles and constitutes valuable diagnostics of beam contents and their mass-changing or charge-changing reactions.[1–3] The same is true for particles confined in Penning traps, where again the large number of orbital or oscillatory motions at fixed frequencies allows single-particle sensitivity and high-precision measurements of motional frequencies,[4–6] often used for high-precision mass spectrometry.[7,8]

The underlying mechanism of all such detectors is described by the Shockley-Ramo theorem, which makes quantitative statements about the electrical currents induced in conductors by charged particles moving above their surface.[9,10] To facilitate particle detection, these signals are picked up by a suited electrode and amplified.

In single-pass situations, repeated signals as discussed above are unavailable and are replaced by a single signal that rises and falls again on the time scale of the particle passing. For small particle numbers, this poses a serious challenge for the amplification stage of any such detector and requires low-noise electronic handling of the initial signal. Devices for nondestructive single-pass detection of charged particles have been used, for example, in the specific context of ion trap experiments[11] and ion implantation,[12] mainly to provide timing information and determine ion currents. The methods presented here allow a simultaneous and nondestructive determination of absolute ion number, bunch length, and particle kinetic energy of an ion bunch from a single-pass measurement.

We demonstrate the capability and applicability of these methods with low-energy bunches of highly charged ions of a single ion species and discuss the obtainable sensitivity of corresponding devices.

II. DETECTION PRINCIPLES

Charged particles above conducting surfaces create induced charges in the conductor, and the amount of charge can be calculated by the standard method of images within electrostatics.[13] For a number of simple geometries, analytic expressions can be found.[14] In general, the fraction of the original charge that becomes induced in an insulated electrode increases with overall electrode area and its proximity to the original charge. Hollow cylinders with a large ratio Z/R of length to radius around the particle trajectory are hence a good choice. When a charged particle passes by the electrode, the induced signal is hence a time-dependent charge signal, changing continuously from zero to a maximum value when the particle is in the electrode centre and back to zero, on the time scale of the passing. This signal can be translated into a voltage that can be amplified and evaluated in order to obtain various information about the passing particles.

A. Induced signal

Nondestructive ion detection is based on the principle of mirror charges induced by a charged particle in a nearby conductive electrode. The magnitude of the induced charge Q_{ind} depends on the ion charge q, the geometry of the pick-up electrode, as well as the ion position relative to the electrode. For single-pass ion detection, the use of a conductive hollow cylinder characterized by its inner radius R and length Z is well suited; see the illustration in Fig. 1. The charge induced by a single ion located at (r_1, z_1) can be expressed by the product of the particle charge q and the so-called geometry function Ξ, i.e.,

$$Q_{ind} = -q \cdot \Xi(r_1, z_1). \tag{1}$$

This geometry function includes all spatial dependences of the device, including the shape of the pick-up electrode and the ion position. The geometry function of an arbitrary electrode geometry has the same shape as the electric potential of that very electrode normalized to unity at the electrode surface.[9] We have calculated the potential and hence the geometry function with the COMSOL Multiphysics™ software.[15] Presently, there is no azimuthal dependency due to the rotational symmetry of the cylinder in use. The geometry function reaches its maximum in the middle of the cylinder at $z = 0$. The value at the maximum depends on the ratio of Z and R. Referring to Fig. 2, there is a minimum electrode length Z for each radius R such that the geometry function takes a value of nearly unity. In particular, increasing the length, a plateau is formed. The voltage U_{ind} induced in the pick-up electrode is connected to its capacitance C by

$$U_{ind} = \frac{Q_{ind}}{C}. \tag{2}$$

This voltage is usually amplified for signal processing by an overall voltage gain of $|\alpha| \gg 1$. The measured voltage is thus given by

$$U = \frac{\alpha \cdot Q_{ind}}{C}. \tag{3}$$

Let us define the sensitivity $S \equiv -\alpha/C$ so that we obtain

$$U = S \cdot q \cdot \Xi(r_1, z_1). \tag{4}$$

The sensitivity is a characteristic property of the charge-counter device including the pick-up electrode and the amplifiers.

For a single ion passing by with a kinetic energy E and corresponding velocity $v = \sqrt{2E/m}$, a time-dependent voltage is induced in the pick-up electrode. Figure 3(a) shows the signal of a single ion passing an electrode which is placed at $z^{(0)} = 2$ m from the position of ion release. The ion has example kinetic energies per charge of 100 eV and 1000 eV, respectively. For a single ion, the induced voltage as a function of time has the same shape as the geometry function, where only the axis is scaled and shifted depending on the ion velocity. Obviously, the induced signal for high energies is located earlier in time and the temporal width is smaller. The amplitude of the signal is independent of the kinetic energy.

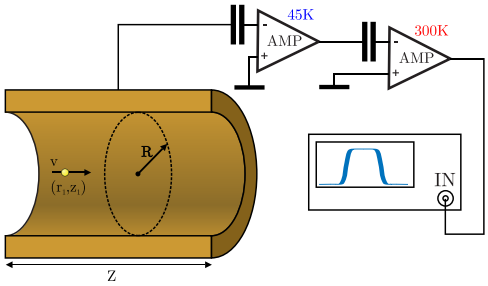

FIG. 1. Detection principle of the single-pass nondestructive charge counter. Charges induced by the passing particles create a corresponding voltage that is amplified by a two-stage amplifier.

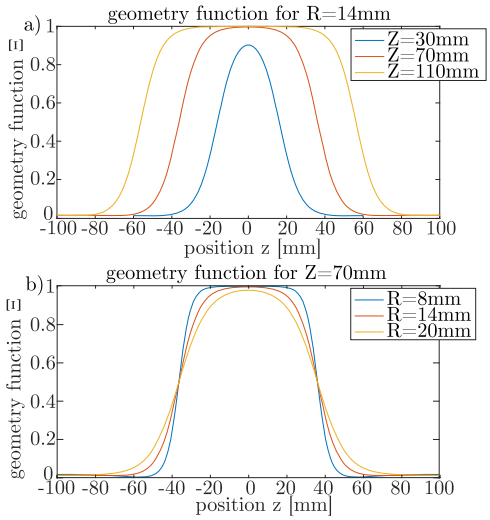

FIG. 2. Dependency of the geometry function Ξ on the geometrical properties of the electrode. (a) Z-dependence for constant radius R = 14 mm and (b) R-dependence for constant length Z = 70 mm. Both diagrams show Ξ along the z-axis for $r_1 = 0$.

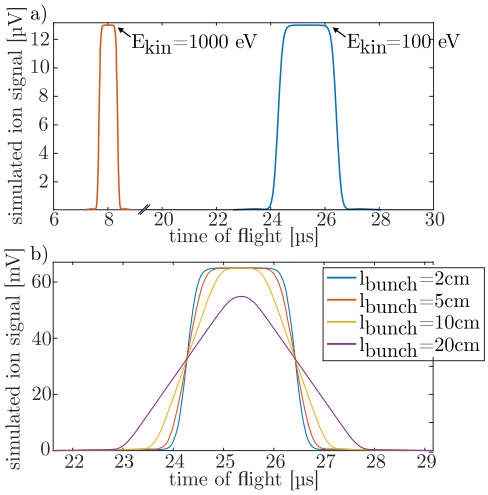

FIG. 3. Output signal of (a) a single passing ion (q = 13e) with different kinetic energies and (b) a bunch of 10 000 ions with different bunch lengths. The sensitivity for the detection system is assumed to be 1 μV/e.

Multiple ions from a pulsed ion source typically have a bunched structure with a certain spatial and hence temporal extent. Here, the induced voltage is the sum of the induced voltages of the individual ions located at positions z_i. The measured signal of a single-species ion bunch of N ions with individual charge q is

$$U_{bunch}(t) = S \cdot q \sum_{i=1}^{N} \Xi(v_i \cdot t - z_i^{(0)}). \tag{5}$$

The signals of long ion bunches show an increased rise time and a decreased length of the plateau [Fig. 3(b)]. For ion bunches longer than the plateau of the geometry function, the plateau in the signal even vanishes completely and the magnitude of the signal decreases. We will use this behavior to estimate the length of the ion bunches.

B. Determination of ion bunch properties from induced signal

The single-pass charge counter is a useful instrument to characterize the most important properties of an ion bunch, namely, its ion number, ion kinetic energy, and the bunch length.

1. Ion number

From the area Ω below the measured voltage curve $U(t)$, the ion number N can be deduced by use of[11]

$$N = \frac{v}{q \cdot L \cdot S} \int U(t)\,\mathrm{d}t = \frac{v}{q \cdot L \cdot S}\,\Omega, \tag{6}$$

where $L \equiv \int_{-\infty}^{\infty} \Xi(z)\mathrm{d}z$ is a characteristic length of the pick-up electrode. For ion bunches shorter than the length of the charge-counter plateau, the ion signal will also establish a plateau, as depicted in Fig. 4. In this case, the geometry function $\Xi(r_i, z_i)$ of all ions is equal to unity. Using this assumption, the number of particles can

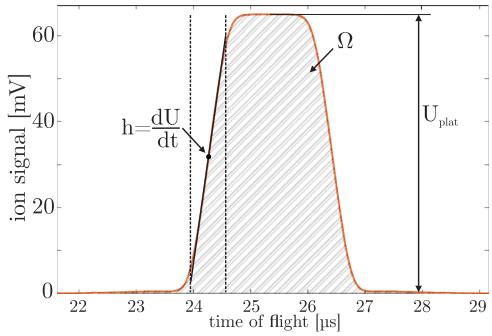

FIG. 4. Simulated signal induced by an ion bunch. The characteristic measures are shown to determine the ion number, the ion velocity, and the bunch length from a single-pass ion signal.

be deduced by rearranging Eq. (5) such that we obtain

$$N = \frac{U_{plat}}{S \cdot q}. \tag{7}$$

This approach to calculate ion numbers has the advantage that knowledge of the ion velocity v is not required.

2. Ion kinetic energy

Equating expressions (6) and (7), one obtains an equation for the ion kinetic energy that is independent from the device's sensitivity,

$$E_{kin} = \frac{1}{2} \cdot m \cdot L^2 \frac{U_{plat}^2}{\Omega^2}. \tag{8}$$

To calculate the kinetic energy, the mass m of the ion species must be known.

3. Ion bunch length

As mentioned above, the slope of the leading edge h is a measure for the bunch length l_b, as depicted in Fig. 4. Assuming an ion bunch with uniformly distributed ions within the bunch of length l_b, the slope of the ion signal can be calculated by

$$\frac{dU}{dt} = \frac{N \cdot S \cdot q \cdot v}{l_b} \cdot [\Xi(z_t + l_b/2) - \Xi(z_t - l_b/2)]. \tag{9}$$

Here, z_t is the time-dependent axial position of the ion bunch centre. In the region where the normalized signal has values between 0.1 and 0.9 (marked by the dashed vertical lines), the slope is nearly constant. If the bunch length is shorter than the rising edge of the geometry function, the slope is independent of the bunch length. This is a lower bound for the bunch length determination. If the bunch is longer, the leading part of the bunch has a geometry function value of unity and the last part has zero. In this case, using $h = dU/dt$ and Eqs. (6) and (7), the bunch length is given by

$$l_b = \frac{U_{plat}^2 \cdot L}{\Omega \cdot h}. \tag{10}$$

Note that Eq. (7) can only be applied when the signal has a plateau. Therefore, the plateau length is an upper limit to measure l_b. If the velocity v is known from another measurement device, the bunch

length l_b can be calculated also in the absence of a plateau and without an upper limitation. In this case, l_b is given by

$$l_b = \frac{v^2 \cdot \Omega}{L \cdot h}. \tag{11}$$

C. Detection electronics

In order to nondestructively detect passing particles, an induced charge is picked up by a suited electrode, and the corresponding voltage U_{ind} as given by Eq. (2) is amplified and read out by an oscilloscope. To this end, the detection electrode is connected to a low-noise amplifier. The overall capacitance C in Eq. (2) then consists of the capacitance C_{pickup} of the pick-up electrode itself, the capacitance C_{cable} of the connecting cable, and the capacitance C_{input} of the amplifier's input; hence, we have $C = C_{pickup} + C_{cable} + C_{input}$. Since any excessive capacitance decreases the signal of interest [see Eq. (2)], care has to be taken in order to minimize the individual contributions to C. Regarding the pick-up electrode, it is advisable to avoid large-surface contacts of the electrode to insulating spacers. Cables need to be kept as short as possible or left away completely, if mounting of the amplifier directly to the pick-up electrode is possible. This may increase the complexity of the mechanical setup but is an inevitable step if highest sensitivity is required. Note that wiring in a vacuum setup with typical line lengths of few meters gravely contributes to the total capacitance since $C_{cable} \gg C_{pickup}$ in most common cases. Thus, the presence of a cable often limits the achievable sensitivity. Finally, the design of the amplifier should support low input capacitance in order not to dominate the resulting value of C.

In general, amplifiers possess three main properties, which are of relevance here:

- the overall voltage gain α
- the intrinsic noise of the amplifier
- the frequency bandwidth f_{band} of the amplifier.

The time structure of the induced ion signal determines the required bandwidth of the amplifier, i.e., the spectral amplification behavior must be chosen in such a way that the Fourier transform of the induced signal falls within the range of sufficient amplification.

The induced voltage U_{ind} is typically of the order of nanovolts, whereas further processing by standard data acquisition systems requires levels of millivolts and above. Hence, amplification by around five to six orders of magnitude is required. The amplifier's intrinsic noise competes with the charge-induced signal, and thus, it is a great challenge if detection of few or even a single particle is envisaged. There are two main contributions to the amplifier's input noise, namely, the amplifier's input voltage noise density e_{na} and the electrical current density i_{na}.[16] These two noise sources can be represented as shown in Fig. 5. Note that i_{na} is a quantity resulting from electrical leakage currents inside the amplifier and also originating from dissipative effects in isolators and at the amplifier input. Both contributions show certain frequency dependences,[16] which have to be taken into account for more detailed considerations.

i_{na} is a real (measurable) electrical AC current which creates an unwanted voltage noise on the total input capacitance C given by

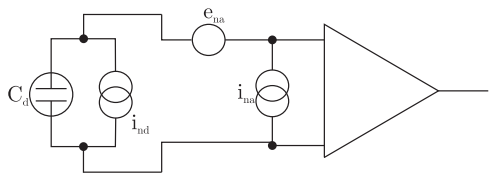

FIG. 5. Schematic of the effective noise source consisting of the two main contributions to the amplifier's input noise, the amplifier's input voltage noise density e_{na}, and the electrical current density i_{na}.

Ohm's law,

$$u_{na}(f) = \frac{i_{na}(f)}{2\pi f \cdot C}. \tag{12}$$

The input voltage noise density $e_{na}(f)$, on the other hand, is a virtual quantity, being derived by dividing the amplifier's output noise density (disregarding i_{na}) by its voltage gain. In good approximation, both contributions are statistically independent; thus, the resulting noise density at the amplifier's input u_{res} is given by $u_{res}^2 = u_{na}^2 + e_{na}^2$. FET (field-effect-transistor) based amplifier technology is the primary choice for charge amplifiers since FET elements are capable of maintaining both small input currents i_{na} as well as small voltage noise e_{na} at moderate input capacitances C_{input}.[16,17]

Figure 6 depicts the internal structure of the developed amplifier. A special customized GaAs (gallium arsenide) FET[18,19] is used as the front-end stage, which is thermalized to the ambient temperature. The FET converts the pickup electrode AC voltage to an output current AC component, and the latter is converted in a room temperature amplifier to voltages again, using a feedback resistor R_f. A μ-controller-regulated PID loop (proportional-integral-derivative loop[16]) keeps the cryogenic FET at a stable operating condition. Cold and warm parts together form a self-calibrating system (CX-4 amplifier), which requires almost no adjustments. In contrast to commercial off-the-shelf GaAs transistors, the FET used here has been especially developed for the purpose of deep-cryogenic operation and very low input voltage and current noise density with $e_{na} \approx 310\ \mathrm{pV}/\sqrt{\mathrm{Hz}}$ at $f = 1$ MHz and $i_{na} \approx 17\ \mathrm{fA}/\sqrt{\mathrm{Hz}}$ at $f = 100$ kHz and $C_{input} = 4.2$ pF at a temperature of 4 K. This noise figure is expected to increase with increasing temperature,[20] indicating optimal use at deep-cryogenic temperatures above carrier-freezeout temperature. It is furthermore designed to require very little operating power of approximately 320 μW, which is quite advantageous in cryogenic systems. This requires a very small bias voltage of about

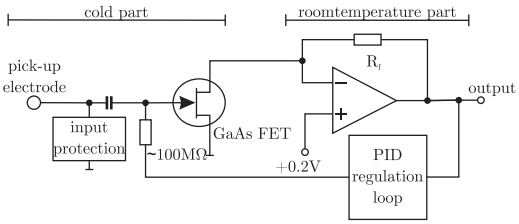

FIG. 6. Internal structure of the developed amplifier. The input side is the pick-up electrode in the cryogenic part of the setup, and the amplified output on the right at room temperature is read by an oscilloscope.

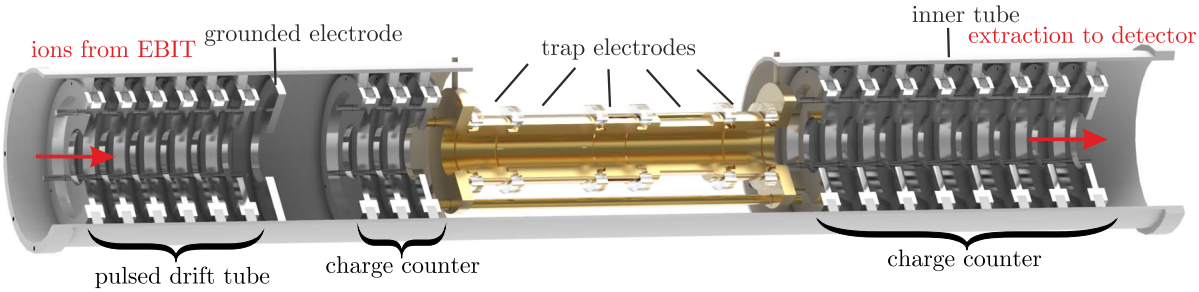

FIG. 7. Section view of the setup inside the magnet bore. Ions from the external source to the left are decelerated in the pulsed drift tube before they pass by the first charge counter and enter the trap. Upon leaving the trap to the detector on the right, the ions pass by the second charge counter which has been used for the below measurements.

0.2 V. For higher temperatures, the AC-resistance of the FET drain-source decreases, which induces a shift of the working point. In the region from 4 K to 300 K, this shift can significantly reduce the total amplification factor for a constant bias voltage.

III. SETUP

The present measurements have been performed in the framework of the HILITE experiment[21] currently operated at GSI, Germany. It features an open-endcap mechanically compensated cylindrical Penning trap placed in the centre of a 6 T superconducting magnet and is cooled to liquid-helium temperature. Adjacent to the trap on either side, a single-pass nondestructive charge counter is installed to detect charged particles entering and leaving the trap, respectively; see central and right-hand side of Fig. 7. The setup is equipped with a dedicated ion source, a commercial EBIT (electron-beam ion trap)[22] placed about 2 m upstream the beamline, which allows us to produce highly charged ions up to Xe^{46+}. A subsequent velocity filter (Wien filter) facilitates selection of a single ion species, i.e., a single charge state. The number of extracted ions is tuned by variation of EBIT parameters such as charge-breeding time and electron energy. The extracted ions' kinetic energy can be tuned by the acceleration voltage U_{acc} at the EBIT and is typically between 1000 V and 2500 V. To perform dynamic ion capture of extracted ions in the trap,[23] the ions are decelerated to an energy of the order of several tens of electronvolts. To that end, a deceleration stage is placed upstream of the trap inside the magnet; see the left-hand side of Fig. 7. It operates as a pulsed drift tube, where the initially positive voltage is switched to negative polarity while the ion bunch is inside the tube. By use of this technique, one can decrease the velocity of the ions significantly. For subsequent axial confinement of the ion bunch, we use the first electrode of the trap (capture electrode). Its initially positive voltage is switched to zero when the long ion bunch approaches. So predominantly, the leading ions are decelerated while the later ions are less affected. Corresponding measurements will be presented in Sec. IV.

IV. MEASUREMENTS AND RESULTS

The present measurements focus on the charge counter to the right-hand side of the trap. This charge counter provides a geometry function with a sufficient plateau which allows application of the presented methods. In order to examine the functionality and possibilities of nondestructive ion detection, bunches of Ar^{13+} ions have been used. The induced ion signal is amplified by the presented two-stage amplifier and recorded by an oscilloscope. An example of a measured signal is shown in Fig. 8 to introduce the quantities used in signal evaluation.

As shown in Sec. II B, an ion bunch of sufficiently small axial extent shows an approximately linear rising edge, a constant plateau with zero slope, and a linear falling edge. We approximate this shape by a trapeze with a base parallel to the time axis. Such a shape is characterized by six numbers. These six parameters are the baseline voltage U_{base}, the plateau voltage U_{plat}, and the four points (A, B, C, D) where the trapeze changes from constant to linear increase or decrease and vice versa. Figure 8 presents the method of this fit and the resulting trapeze for an example signal. The key parameters of interest are extracted from the fit result. The baseline signal U_{base} and the plateau voltage U_{plat} are directly given by the fit. However, using the top of the trapeze to determine U_{plat} tends to underestimate the plateau voltage. Therefore, the plateau voltage is determined with the acquired width $\Delta t = (t_C - t_D)$ of the top of the trapeze as a reference. U_{plat} is the mean of the signal $U_{signal}(t)$ in a region with a width of 60% of Δt around the centre of the trapeze. This reduces the errors caused by the rounded corners of the signal at C and D. Following Eq. (8), for the determination of the kinetic energy, the area Ω is calculated by numerical integration of the acquired signal $U_{signal}(t)$

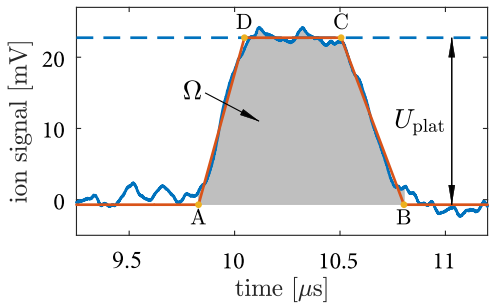

FIG. 8. Charge-counter signal $U_{signal}(t)$ of an Ar^{13+} ion bunch with an acceleration voltage of 984 V with 64 averages. One bunch consists of about 3200 ions. To analyze the signal, a trapeze is fitted to the trace. It is shown in orange. The four yellow points define the trapeze. The marked area of the signal is determined by numerical integration from A to B.

between times A and B,

$$\Omega = \int_{t_A}^{t_B} (U_{signal}(t) - U_{base})\mathrm{d}t.$$

A high signal-to-noise ratio is crucial to detect small numbers of ions. For repeatable measurements, averaging is an expedient solution. This technique reduces the noise proportionally to the square root of the number of averages.

For single-pass experiments with nonconstant operation conditions, this is not a feasible option. Instead, the noise can be reduced by use of a software-based low-pass filter, considering that the filter's cut-off frequency does not affect the important parts of the signal. When an upper limit of the velocity is known, Eq. (5) can be used to calculate the expected spectrum of an ion bunch, as obtained by the Fourier transform of the time-dependent ion signal. For the present evaluation, the cut-off frequency of the filter was set to f_{cut} = 4 MHz. Figure 9 compares the effects of averaging and the low-pass filter. Obviously, both strategies have a similar effect. As the computational effort for signal filtering is moderate, this technique will be preferred here.

A. Nondestructive energy measurement

With the presented signal analysis method, the kinetic energy of an ion bunch can be directly determined from an acquired charge-counter signal. To test this method, bunches of Ar^{10+} and Ar^{15+} ions have been used. The kinetic energy of each bunch can be varied by changing the acceleration voltage (U_{acc}) of the EBIT. We have acquired the charge-counter signals for acceleration voltages between 1000 V and 2200 V. The measured signals are single-pass traces of one ion bunch without averaging and with a digital filter as described above. Figure 10 shows the result of this measurement with a comparison to the expected value. The uncertainty of the kinetic energy is deduced from the uncertainty of the trapeze fit. Obviously, the experimentally determined energy values are in good agreement with the expected energies.

B. Ion number calibration measurement

For a determination of absolute ion numbers by use of Eq. (6) or Eq. (7), the sensitivity S of the detection system needs to be known

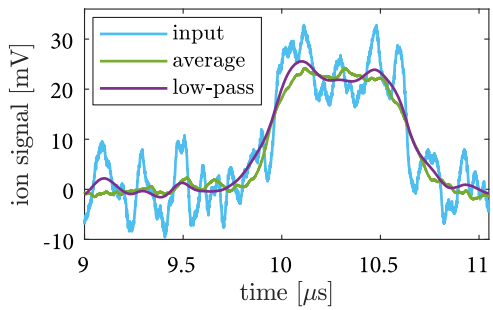

FIG. 9. Possible methods to reduce the noise in a charge counter signal. The diagram shows the signal of Ar^{13+} at 984 V acceleration voltages. One can see that both averaging and filtering reduce the noise. The signal was filtered with a fourth-order digital low-pass filter with f_{cut} = 4 MHz.

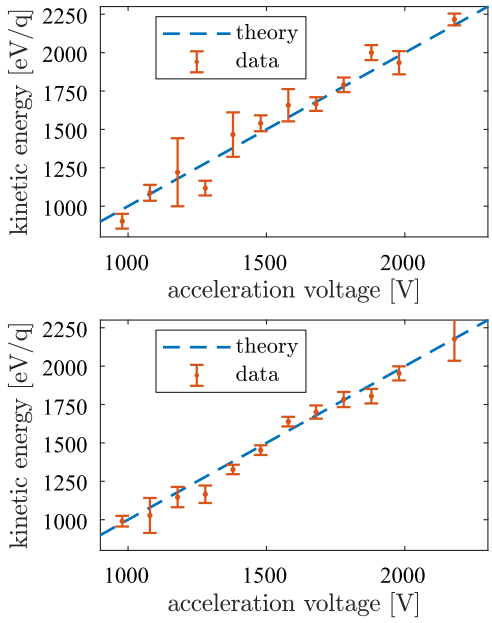

FIG. 10. Nondestructive single-pass kinetic energy measurement of Ar^{10+} (top) and Ar^{15+} (bottom) ion bunches using a charge counter. Each data point corresponds to the filtered signal of a single ion bunch. The x-axis shows the applied acceleration voltage U_{acc}, and the y-axis is the measured energy per charge. The dashed line shows the theoretical kinetic energy that corresponds to the acceleration voltage of the EBIT. The errors are calculated based on the errors estimated at the trapeze-fit procedure.

for the actual experimental conditions. We have chosen two different approaches to determine the sensitivity of our charge counter—a calibration evaluating the plateau voltage (U_{plat}) and a calibration using the area Ω under the ion signal. The calibration measurements have been performed with a Faraday cup as a reference ion-counting detector. An ion bunch impacting the Faraday cup causes a current $I_{FC}(t)$ from the Faraday cup. The current is amplified using a current amplifier with a voltage gain of α_{FC} = (1.00 ± 0.01) V/μA. The resulting voltage signal of the Faraday cup $U_{FC}(t)$ is recorded with an oscilloscope. From this signal, the number of ions N_{FC} can be deduced by use of

$$N_{FC} = \frac{1}{q \cdot \alpha_{FC}} \int U_{FC}(t)\mathrm{d}t, \tag{13}$$

where q is the charge of the ion species. The area of the recorded Faraday cup signal is determined by numeric integration. The integration bounds are set where the signal falls to 3% of the maximum value.

For calibration measurements, we have chosen Ar^{15+} ions because it is the highest argon charge state that can be produced in sufficient amounts. To calibrate the detector, ion bunches with different total numbers of ions have been used. This has been accomplished by variation of the breeding time of the EBIT. The corresponding charge-counter signals have been analyzed with the presented method to extract the area and the plateau signal. Figure 11 shows the result of this calibration measurement. Using Eqs. (6), (7),

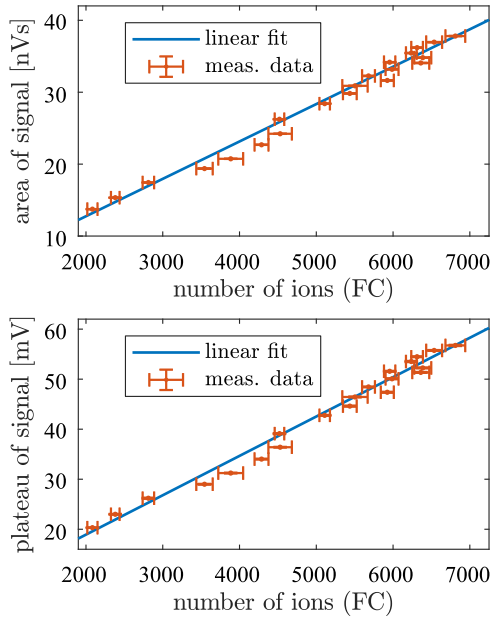

FIG. 11. Results of the calibration measurement of the charge counter with the Faraday cup. To produce ion bunches with different ion numbers, the breeding time was varied between 1000 ms (minimum number of ions) and 4000 ms (maximum number of ions). Each data point results from the averaged signal of 32 measured ion bunches. The upper diagram shows the area Ω of the charge counter signal over the measured ion number of the Faraday cup using Eq. (13). The slope of the linear fit is m_{area} = (5.08 ± 0.15) × 10^{-12} Vs/ion. The lower diagram shows the plateau voltage of the charge counter signal over the ion number from the FC. The slope of the linear fit here is m_{plat} = (7.82 ± 0.22) μV/ion.

and (13), two expressions for the sensitivity can be extracted. One for both linear slopes m_{area} and m_{plat} in Fig. 11,

$$S = \frac{v}{q \cdot L} m_{area}, \qquad S = \frac{1}{q} m_{plat}.$$

The resulting calibrated sensitivities $S \equiv -\alpha/C$ are shown in Table I. For comparison, the capacitance C and the total voltage gain α have been measured at room temperature, resulting in C = (116.1 ± 0.1) pF and α = −329(1) ± 1, leading to a sensitivity of S = (455.9 ± 0.57) nV/e, slightly below the measured sensitivity at 100 K. A measurement at a temperature of 4 K yields a voltage gain of α = −2400 and a corresponding sensitivity of S = 3326 nV/e. A temperature dependence of the electronic noise and hence of the detector sensitivity can be expected[20] as it was mentioned already in Sec. II C.

TABLE I. Calibration results of the charge counter at a temperature of 100 K. The sensitivity $S \equiv -\alpha/C$ is given in units of e to illustrate the output signal voltage at the oscilloscope per elementary charge. Both results are in good agreement.

Measurement	S (nV/e)
From area	524 ± 15
From plateau	521 ± 15

C. Ion deceleration and ion bunching

As discussed above, the ions from the EBIT ion source have initial kinetic energies of the order of kiloelectronvolt. Therefore, the ions need to be decelerated before they can be captured in the trap. In addition, we use one electrode to compress the ion bunch in the axial direction by applying a positive voltage which is switched zero when the ions approach the electrode. The properties of the ion bunches (ion number, kinetic energy, and bunch-length) are again determined by use of the charge counter. Ion bunches with a length of less than 150 mm can be fully characterized with respect to the number of ions, kinetic ion energy, and bunch length by use of the charge counter. This is true since only in this case a plateau in the signal occurs, which is necessary for the described evaluation techniques.

For the present deceleration measurements, Ar^{13+} ions with a kinetic energy of 979 eV (as controlled by the velocity filter) have been used. We have recorded the charge counter ion signal; see Fig. 12(a). The presented evaluation of the signal gives a kinetic energy of E_{kin} = (968 ± 30) eV as expected and an ion number of N = 3400 ± 30. For deceleration, we have set our pulsed drift tube to a potential of +400 V and switched it to −400 V when the ion bunch is located inside of the electrode. The charge counter signal of the thus

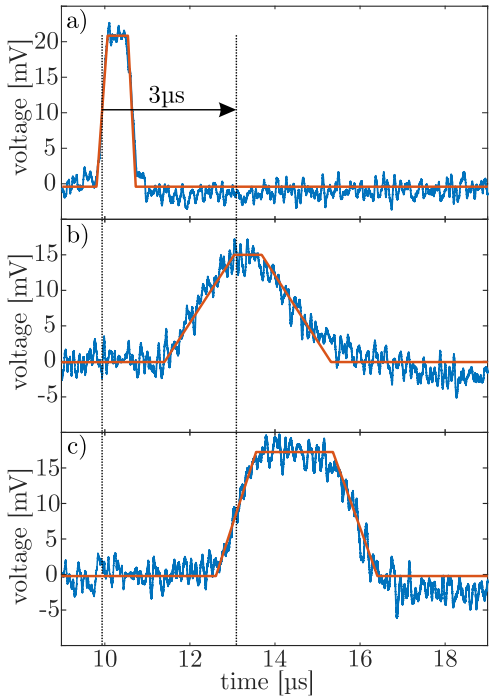

FIG. 12. Ion bunch properties of (a) an undecelerated ion bunch with a kinetic energy of E = 979 eV, (b) a bunch decelerated by a pulsed-drift tube with ΔU_{PDT} = 800 V, and (c) a compressed ion bunch after deceleration with a remaining kinetic energy of 87 eV. The length of the ion bunch is at the lower detection limit.

decelerated ions is shown in Fig. 12(b), where the time shift of about 3 μs indicates the deceleration. The signal also is broadened, which is caused by the ion deceleration. As the plateau is not pronounced clearly, a quantitative evaluation of the ions' kinetic energy, number, and bunch-length could not be performed. The short plateau is a strong indicator for an ion bunch with an axial extend of about 150 mm, which is the upper detectable limit.

To axially compress the ion bunches, we use the first trap electrode along the direction of the ion motion. This electrode is set to 95 V and switched to 0 V within about 270 ns, when the ion bunch approaches the electrode. In this case, the first faster ions are decelerated, while the slower ions behind are affected less by the electrode's potential resulting in a compression of the ion bunch. This process can be verified by the recorded ion signal in Fig. 12(c). Here, the plateau again is well pronounced with a sufficient length. From this, the ion energy and the ion number are determined to be (87 ± 5) eV and $N = (2500 \pm 70)$, respectively. From the slope of the leading edge of the signal, we find the bunch length to be about 50 mm or less as 50 mm is the minimum detectable limit.

D. Detection limit

The minimum number of detectable ions is determined by the noise level and the signal voltage. For N ions with charge q, the maximum signal voltage is given by

$$U_{max} = q \cdot N \cdot S.$$

The signal-to-noise ratio η is given by the maximum signal amplitude divided by the noise amplitude. Based on this definition, for a chosen value of η, the minimum number of detectable ions can be estimated in terms of the input noise density e_{na},

$$N_{min} = \frac{\eta \cdot C}{q} \cdot e_{na} \cdot \sqrt{f_{band}}.$$

At a frequency of 1 MHz and a temperature of 100 K, the measured input noise density is $e_{na} = 1450\ \mathrm{pV}/\sqrt{\mathrm{Hz}}$. Together with the bandwidth of the amplifier of $f_{band} = 4$ MHz, the minimum number of detectable Ar^{13+} ions for $\eta = 3$ is

$$N_{min} = 480.$$

In contrast, at cryogenic temperatures of $T = 4$ K and without an external magnetic field, the input noise density has been measured to be $e_{na} = 310\ \mathrm{pV}/\sqrt{\mathrm{Hz}}$. This results in a detection limit of

$$N_{min} = 95$$

ions of Ar^{13+}. The higher value of $N_{min} = 480$ above is mainly attributed to thermal noise effects at the current experiment temperature of about 100 K. A possible influence of the external magnetic field in the experiment requires closer investigation. For a detection electrode with an optimized capacitance which is equal to the input capacitance of the amplifier ($C = 2 \cdot C_{input} = 8.4$ pF), the detection limit at a temperature of 4 K is given by

$$N_{min} = 7$$

ions of Ar^{13+}. This means that with the current amplifier and an optimized detection electrode, 91 elementary charges could be detected with a signal-to-noise ratio of $\eta = 3$. Hence, single-pass detection of single bare uranium ions may become possible.

V. SUMMARY AND OUTLOOK

We have presented the concept, implementation, and characterizing measurements with a single-pass nondestructive ion counter, which is capable of measuring ion kinetic energy, ion number, and the length of ion bunches from a single-pass signal. By a calibration of the sensitivity of the device, absolute ion numbers can be determined. The analysis procedure does not require high computational effort to infer the desired ion bunch parameters from the acquired signal. The accuracy of the measurement of ion number and ion energy is limited by the experimental conditions of the setup. In the present configuration, at a temperature of 100 K, the minimum detectable number of Ar^{13+} ions in a bunch is about 480, as follows from the measured input noise density e_{na}. At a temperature of 4 K, this figure is about 95. These numbers result from the capacitance of the pick-up electrode, the input voltage noise density, and the amplification bandwidth. We intend to optimize this kind of device with respect to the minimum number of detectable charges by a reduction in the capacitance via an optimized geometry. Additionally, a new generation of cryocooled radio-frequency amplifiers with reduced input noise is being developed with the aim of achieving single-charge sensitivity.

ACKNOWLEDGMENTS

This work has been in part supported by the European Commission's Horizon 2020 Programme No. 721559 AVA.

REFERENCES

[1] J. Borer, P. Bramham, H. G. Hereward, K. Hübner, W. Schnell, and L. Thorndahl, in *Proceedings of the IXth International Conference on High Energy Accelerators* (Stanford, 1974), p. 53.
[2] F. Nolden, P. Hülsmann, Y. A. Litvinov, P. Moritz, C. Peschke, P. Petri, M. S. Sanjari, M. Steck, H. Weick, J. X. Wu *et al.*, Nucl. Instrum. Methods Phys. Res., Sect. A **659**, 69 (2011).
[3] D. Shubina, R. B. Cakirli, Y. A. Litvinov, K. Blaum, C. Brandau, F. Bosch, J. J. Carroll, R. F. Casten, D. M. Cullen, I. J. Cullen *et al.*, Phys. Rev. C **88**, 024310 (2013).
[4] D. J. Wineland and H. G. Dehmelt, J. Appl. Phys. **46**, 919 (1975).
[5] L. S. Brown and G. Gabrielse, Rev. Mod. Phys. **58**, 233 (1986).
[6] S. Sturm, A. Wagner, M. Kretzschmar, W. Quint, G. Werth, and K. Blaum, Phys. Rev. A **87**, 030501 (2013).
[7] K. Blaum, Phys. Rep. **425**, 1 (2006).
[8] M. Block, *Fundamental Physics in Particle Traps* (Springer, 2014), pp. 223–251.
[9] W. Shockley, J. Appl. Phys. **9**, 635 (1938).
[10] S. Ramo, Proc. IRE **27**, 584 (1939).
[11] S. Schmidt, T. Murböck, Z. Andelkovic, G. Birkl, W. Nörtershäuser, S. Stahl, and M. Vogel, Rev. Sci. Instrum. **86**, 113302 (2015).
[12] P. Räcke, D. Spemann, J. W. Gerlach, B. Rauschenbach, and J. Meijer, Sci. Rep. **8**, 9781 (2018).
[13] J. D. Jackson, *Classical Electrodynamics* (AAPT, 1999).
[14] D. F. A. Winters, M. Vogel, D. M. Segal, and R. C. Thompson, J. Phys. B: At., Mol. Opt. Phys. **39**, 3131 (2006).
[15] COMSOL AB, Stockholm, Sweden, COMSOL Multiphysics® v. 5.2.
[16] P. Horowitz and W. Hill, *The Art of Electronics* (Cambridge University Press, 1989).
[17] H. Spieler, *Semiconductor Detector Systems* (Oxford University Press, 2005), Vol. 12.
[18] Q. Dong, Y. Liang, D. Ferry, A. Cavanna, U. Gennser, L. Couraud, and Y. Jin, Appl. Phys. Lett. **105**, 013504 (2014).

[19]Y. X. Liang, Q. Dong, M. C. Cheng, U. Gennser, A. Cavanna, and Y. Jin, Appl. Phys. Lett. **99**, 113505 (2011).
[20]Y. Jin, Q. Dong, Y. X. Liang, A. Cavanna, U. Gennser, L. Couraud, and C. Ulysse, J. Phys.: Conf. Ser. **568**, 032009 (2014).
[21]M. Vogel, W. Quint, G. G. Paulus, and T. Stöhlker, Nucl. Instrum. Methods Phys. Res., Sect. B **285**, 65 (2012).
[22]G. Zschornack, F. Grossmann, U. Kentsch, V. P. Ovsyannikov, M. Schmidt, and F. Ullmann, Nucl. Instrum. Methods Phys. Res., Sect. B **235**, 514 (2005).
[23]H. Schnatz, G. Bollen, P. Dabkiewicz, P. Egelhof, F. Kern, H. Kalinowsky, L. Schweikhard, H. Stolzenberg, and H.-J. Kluge, Nucl. Instrum. Methods Phys. Res., Sect. A **251**, 17 (1986).